particles

MDPI

Review

Progress on the Proton Decays of $A \sim 20$ Nuclei Around the Proton Drip Line

Lei Ni, Yu Jin, Hui Hua * and Zhihuan Li

School of Physics and State Key Laboratory of Nuclear Physics and Technology, Peking University, Beijing 100871, China; nileini@126.com (L.N.); yuu@pku.edu.cn (Y.J.); zhli@pku.edu.cn (Z.L.)
* Correspondence: hhua@pku.edu.cn

Abstract

Experimental studies on the spontaneous nucleon emission in nuclei around the drip line enable us to explore new isotopes or resonant states, and to reveal exotic structures and decay properties of nuclei located far from the β stability line; consequently, they are of critical importance for probing limits of nuclear stability and understanding nucleon–nucleon interactions under extreme conditions of isospin asymmetry. With the radioactive isotope beam ^{20}Mg provided by the National Superconducting Cyclotron Laboratory at Michigan State University, we studied the proton decays of nuclei around the proton drip line at $A \sim 20$ mass region. Complete-kinematics measurements were performed for proton decays of one-proton resonant states in ^{18}Na, two-proton resonant states in ^{20}Mg, three-proton resonant states in ^{21}Al, and four-proton resonant states in ^{18}Mg, yielding decay energy spectra for all four nuclei. With the invariant mass method, the ground state of ^{18}Na was firmly identified, clarifying previous ambiguities of its position. The isotope ^{18}Mg, which is located two neutrons beyond the proton drip line, was experimentally observed for the first time. Multi-body correlation analysis of emitted protons from ^{20}Mg, ^{21}Al, and ^{18}Mg, combined with Monte Carlo simulations, reveals that the identified resonant states in ^{20}Mg and ^{21}Al predominantly decay via two and three sequential steps of $1p$ emission, respectively, whereas the ^{18}Mg ground state decays mainly through a two-step cascade of prompt $2p$ emission.

Keywords: proton drip line; proton decay; invariant mass method; resonant state

1. Introduction

A nucleus is a quantum many-body system composed of protons and neutrons, tightly bound by the strong interaction. For nuclei increasingly distant from the β-stability line, the binding energy of the outermost nucleons gradually decreases, reaching zero for the last proton (or neutron) on the proton (or neutron) drip line. In the vicinity of the drip line, the outermost nucleons are weakly bound or unbound. Consequently, some excited states of bound nuclei inside the drip line, as well as the ground states of unbound nuclei beyond it, can decay via spontaneous nucleon emission.

As early as the 1960s, it was predicted that nuclei near the proton drip line might undergo spontaneous decay by emitting one or two protons [1,2]. Beginning in the 1970s, experiments successively discovered that the ground states of many odd-Z nuclei exhibit one-proton radioactivity [3,4]. Constrained by energy and momentum conservation, the decay kinematics of one-proton emission can be fully determined. As the number of emitted protons increases, although the correlations among the decay products become complex,

Check for updates

Academic Editor: Joachim Enders

Received: 26 February 2026
Revised: 26 March 2026
Accepted: 27 March 2026
Published: 1 April 2026

Copyright: © 2026 by the authors. Licensee MDPI, Basel, Switzerland. This article is an open access article distributed under the terms and conditions of the Creative Commons Attribution (CC BY) license.

multi-proton decay reveals many novel phenomena [5,6]. The experimental measurement of momentum and angular correlations among the emitted protons provides information on nucleon wave functions and nucleon–nucleon interactions, which is crucial for understanding nuclear structure under extreme conditions of isospin asymmetry. To date, ground-state two-proton decay has been experimentally observed in ^{6}Be, ^{11}O, ^{12}O, ^{15}Ne, ^{16}Ne, ^{19}Mg, ^{30}Ar, ^{45}Fe, ^{48}Ni, ^{54}Zn, and ^{67}Kr [4,7–12]. With the continued expansion of the nuclear chart beyond the proton drip line, five ground-state three-proton emitters (^{7}B [13], ^{13}F [14], ^{17}Na [15], ^{20}Al [16], and ^{31}K [17]), two ground-state four-proton emitters (^{8}C [18] and ^{18}Mg [19]), and one ground-state five-proton emitter (^{9}N [20]) have been identified in recent years.

With the accumulation of experimental results, many related theoretical developments have been made in recent years regarding various aspects of proton decay, including the identification of decay candidates, the exploration of decay mechanisms, and the investigation of the structure of proton emitters [6]. Using a self-consistent Hartree-Fock-Bogoliubov (HFB) approach, Ref. [21] explored candidates for ground-state 2p emitters, suggesting that nearly all elements between Ar and Pb could have isotopes decaying via 2p emission. Moreover, a fundamental challenge remains in understanding the decay mechanisms and structure of nuclei near the proton drip line. For weakly bound and unbound nuclei, an appropriate treatment of resonant state and continuum effects is essential. In contrast to the conventional shell model, the Gamow shell model (GSM) [22] and the Gamow coupled-channel (GCC) method [23] provide a more suitable framework for describing exotic phenomena in these open quantum systems. Employing the Berggren ensemble [24], these approaches offer a unified description of the interplay between bound states, resonances, and scattering states within a many-body framework. In recent years, these theoretical models have been successfully applied to describe the decay mechanisms and structure of many proton emitters [12,19,20,25–28].

This article reviews our recent experimental studies of proton decay of nuclei around the proton drip line at $A \sim 20$ mass region [19,29–31]. Complete-kinematics measurements were performed for proton decays of one-proton resonant states in ^{18}Na, two-proton resonant states in ^{20}Mg, three-proton resonant states in ^{21}Al, and four-proton resonant states in ^{18}Mg, yielding decay energy spectra for all four nuclei with the invariant mass method. The experiment enabled the identification of the ground state of ^{18}Na and led to the first observation of the isotope ^{18}Mg. Furthermore, by analyzing the correlations in the subsystem decay energy spectra of ^{20}Mg, ^{21}Al and ^{18}Mg, their multi-proton decay mechanisms were discussed.

2. Experiment

The experiment was performed at the National Superconducting Cyclotron Laboratory (NSCL) at Michigan State University. The experimental setup is depicted in Figure 1. A radioactive beam of ^{20}Mg was produced using the Coupled Cyclotron Facility (CCF) and the A1900 fragment separator at NSCL [32,33]. The beam had an energy of E/A = 103 MeV/u, an intensity of 5600 pps, and a purity of 31%. Resonant states of various nuclei near the proton drip line, including ^{18}Na, ^{20}Mg, ^{21}Al, and ^{18}Mg, were populated via different reactions of the ^{20}Mg beam with a ^{9}Be target. These resonant states decayed promptly within the ^{9}Be target, emitting one or more protons along with the residues. The proton decay processes of these resonances were investigated experimentally by performing coincidence measurements of the decay products.

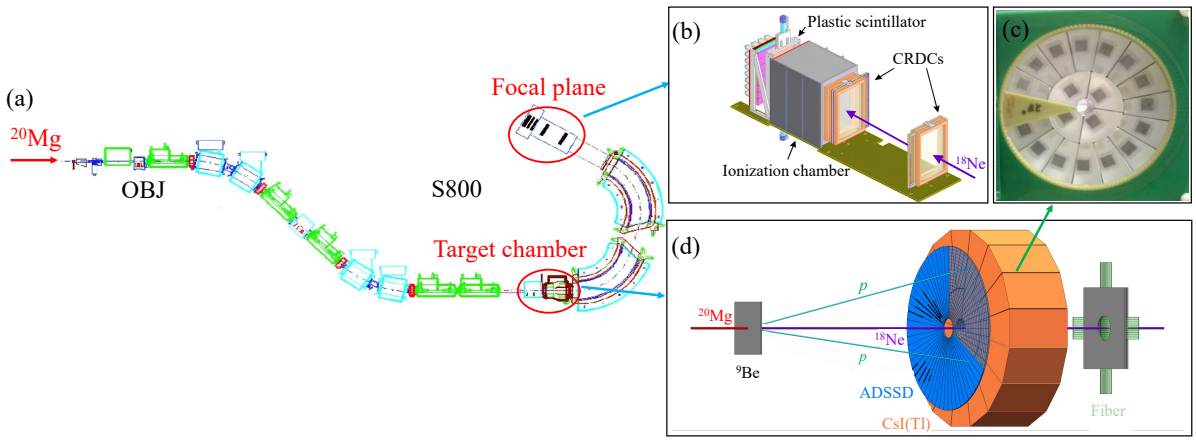


Figure 1. Experimental setup. (**a**) S800 spectrograph [34]; (**b**) S800 focal plane detector array [35]; (**c**) Annular CsI(Tl) detector array; (**d**) Reaction target and target chamber detector array.

The emitted protons were detected by a ΔE–E telescope system, which consisted of an annular double-sided silicon strip detector (ADSSD) and an annular CsI(Tl) array. This system provided information on the position, energy and particle identification of the decay protons. The majority of the residues, focused around zero degrees, passed through a 10-mm diameter central hole of the ΔE–E telescope array. Their positions were determined by a position-sensitive scintillating fiber array. Subsequent to this, the residues entered the S800 spectrograph for particle identification and energy measurement [36,37].

3. Results and Discussion

3.1. One-Proton Decay of ^{18}Na

^{18}Na, with 11 protons and 7 neutrons, is located two neutron steps beyond the proton drip line and decays by emitting one proton to the bound nucleus ^{17}Ne. Zerguerras et al. first observed ^{18}Na experimentally using a ^{20}Mg beam impinging on a ^{9}Be target via nucleon knockout reaction [38]. Through invariant mass reconstruction of ^{17}Ne + 1p events, two peaks at E_T = 0.42(17) and 1.27(17) MeV were observed in the decay energy spectrum, both of which were suggested as possible ground state of ^{18}Na [38]. Subsequently, Assié et al. investigated the low-lying resonant states of ^{18}Na using the resonant-elastic-scattering reaction of ^{17}Ne + 1p [39,40]. By performing an R-matrix analysis of the measured excitation function, they reported four resonant states in ^{18}Na with decay energies of E_T = 1.552(5), 1.842(40), 2.030(20), and 2.084(5) MeV, and spin-parities of 2^-, 0^-, 1^-, and 3^-, respectively. Around the same time period, Mukha et al. studied ^{18}Na using a ^{20}Mg beam on a ^{9}Be target, employing nucleon knockout reaction and the decay-in-flight decay method [41]. By analyzing the p-^{17}Ne angular correlations from 2p decay events of low-lying states in ^{19}Mg, two resonant states in ^{18}Na at E_T = 1.23(15) and 1.55(7) MeV, with spin-parities of 1^- and 2^-, respectively, were determined. The first 1^- resonance was considered a candidate for the ground state of ^{18}Na, while the second corresponded to the 2^- excited state at E_T = 1.552(5) MeV reported in Refs. [39,40]. No resonant structure corresponding to the 1p peak at E_T = 0.42(17) MeV reported in Ref. [38] was observed in Ref. [41]. More recently, Charity et al. populated resonant states of ^{18}Na via the proton transfer reaction with a ^{17}Ne beam and a ^{9}Be target [42]. Two excited states at E_T = 1.527(25) and 2.085(23) MeV with spin-parities of 2^- and 3^-, respectively, were identified, while the ground state of ^{18}Na was not observed in this invariant-mass study. To unambiguously determine the exact position of the ground state of ^{18}Na, we populated its resonant states via the nucleon knockout reaction of a ^{20}Mg beam on a ^{9}Be target.

Figure 2a displays the invariant mass spectrum reconstructed from all the ^{17}Ne + 1p events in the present work [29]. The corresponding detection efficiency, determined via Monte Carlo simulations, is approximately 29%. A clear resonant peak is seen at $E_T \approx 0.4$ MeV, consistent with the $E_T = 0.42(17)$ MeV candidate for the ground state of ^{18}Na reported in Ref. [38] using the same reaction. However, further coincidence analysis indicates that the measured ^{17}Ne + 1p events may originate not only from the one-proton decay of ^{18}Na resonant states but also from contamination of the two-proton decay of ^{19}Mg, produced by the knockout reaction of ^{20}Mg [30,43]. In the two-proton decay process of ^{19}Mg, it is possible that only one of the two emitted protons is detected by both the ADSSD and CsI(Tl) detectors, while the other proton is missed. This also leads to the ^{17}Ne + 1p coincidence events, thereby constituting contamination in the true decay spectrum of ^{18}Na. By randomly selecting one proton from ^{17}Ne + 2p events to construct a ^{17}Ne + 1p spectrum, the contamination spectrum due to one-proton loss can be approximated, as shown by the gray data points in Figure 2a. For the prompt 2p decay of the ^{19}Mg ground state ($E_T \approx 0.8$ MeV), the probability is maximized when the two protons share the decay energy equally, resulting in a peak around $E_T \approx 0.4$ MeV in the ^{17}Ne + 1p spectrum. Since the ground state decay of ^{19}Mg does not proceed through an intermediate state of ^{18}Na, it is confirmed that the peak at $E_T \approx 0.4$ MeV observed in our experiment and in Ref. [38] actually originates from the prompt 2p decay of the ^{19}Mg ground state, rather than from the one-proton decay of an ^{18}Na resonant state.

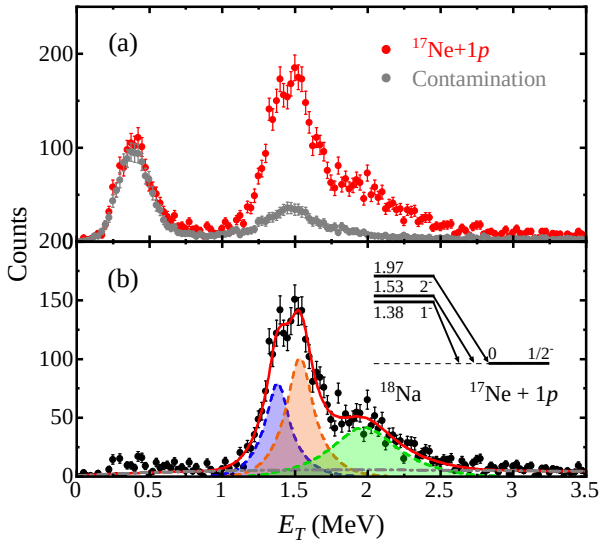


Figure 2. Decay energy spectra for (**a**) all detected ^{17}Ne + 1p events (red points), and (**b**) ^{17}Ne + 1p events after subtracting the contamination from the 2p decay of ^{19}Mg [29]. The grey spectrum in (**a**) indicates the contamination from ^{19}Mg decay, which is estimated from invariant-mass reconstruction of the two possible ^{17}Ne + 1p subevents within each ^{17}Ne + 2p event. The solid-red curve in (**b**) shows the fitted spectrum, which includes the contributions from individual states (dashed curves) and a smooth background (dashed-dotted-grey curve). The inset shows the decay paths of the three resonant states in ^{18}Na.

After subtracting the contamination from the 2p decay of ^{19}Mg, the decay energy spectrum of ^{18}Na is presented in Figure 2b [29]. The experimental resolutions (FWHM) at the centroids of the three observed peaks are 200, 220, and 250 keV, respectively. The spectrum was fitted using Breit-Wigner intrinsic line shapes generated by Monte Carlo simulations. The decay energies E_T and intrinsic widths Γ for the three resonant states of ^{18}Na, including the ground state, were obtained. The one-proton decay energy of the ^{18}Na ground state is determined to be 1.38(2) MeV, consistent with the previously reported ground-state candi-

dates at 1.27(17) MeV [38] and 1.23(15) MeV [41], with the new result significantly reducing the uncertainty in the ^{18}Na ground-state mass. The second resonant state has a decay energy of E_T = 1.53(2) MeV and a width of $\Gamma < 0.04$ MeV, matching the 2^- state in ^{18}Na reported in Refs. [39,40] at E_T = 1.552(5) MeV with Γ = 0.005(3) MeV, and also consistent with results in Refs. [41,42]. The third resonance at E_T = 1.97(2) MeV with Γ = 0.32(4) MeV may arise from the combined contributions of all the three known resonant states in this energy region (0^-_1, 1^-_2, and 3^-_1) [39,40], with its width closest to the intrinsic width of the 0^-_1 state. As shown in the inset of Figure 2b, all three resonant states decay to the ground state of ^{17}Ne.

3.2. Two-Proton Decay of ^{20}Mg

As a nucleus located at the proton drip line, only the ground state (0^+_1) and the first excited state (2^+_1) of ^{20}Mg are bound. Two resonant structures above its two-proton separation threshold (S_{2p} = 2.418(2) MeV [44]), at excitation energies of E^* = 3.7(2) and 5.37(2) MeV, have been reported in previous study using the ^{20}Mg(d,d') reaction [45]. The first relatively wide resonant peak was suggested to potentially result from an overlap of the 4^+_1 and 2^+_2 resonant states in ^{20}Mg [45]. In the present experiment, the two-proton resonant states of ^{20}Mg were populated via projectile inelastic-excitation reaction. The decay energy spectrum of ^{20}Mg, reconstructed from the measured ^{18}Ne + 2p events, is shown in Figure 3 [30]. The associated detection efficiency is approximately 16%. By fitting the experimental spectrum, the energies and widths of four resonant states in ^{20}Mg were determined. With improved resolution, the new results clearly separate the overlapping resonant structure previously observed near E^* = 3.7(2) MeV in Ref. [45]. Through comparison with shell model (SM) calculations from Ref. [45] and the level structure of the mirror nucleus ^{20}O [46], the first two resonances in Figure 3 were assigned as the 4^+_1 and 2^+_2 states of ^{20}Mg, with decay energies of E_T = 0.930(2) and 1.468(5) MeV, respectively [30]. The corresponding experimental resolutions (FWHM) for these two states are 210 keV and 260 keV.

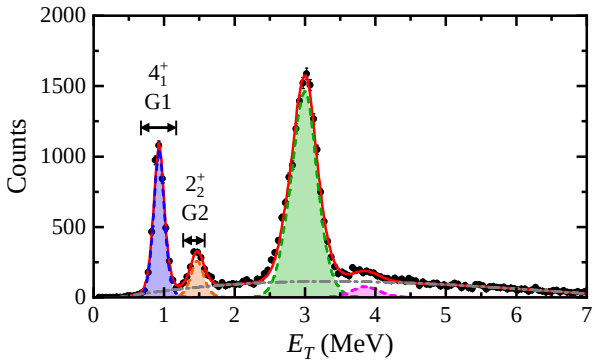


Figure 3. Decay energy E_T spectrum for all detected ^{18}Ne + 2p events [30]. The solid-red curve shows the fitted spectrum along with the contributions of each state (dashed curves) and the smooth background (dashed-dotted-grey curve).

To investigate the 2p decay paths of the 4^+_1 and 2^+_2 states in ^{20}Mg, we analyzed their ^{18}Ne + 1p subsystem decay spectra, which are selected using the gates G1 and G2 indicated in Figure 3. The smooth background under the two gates constitutes 10.7% and 31.0% of the total events, respectively. The influence of the higher background level was taken into account in the decay path analysis for the 2^+_2 state. The results are shown in Figure 4a and Figure 4b, respectively.

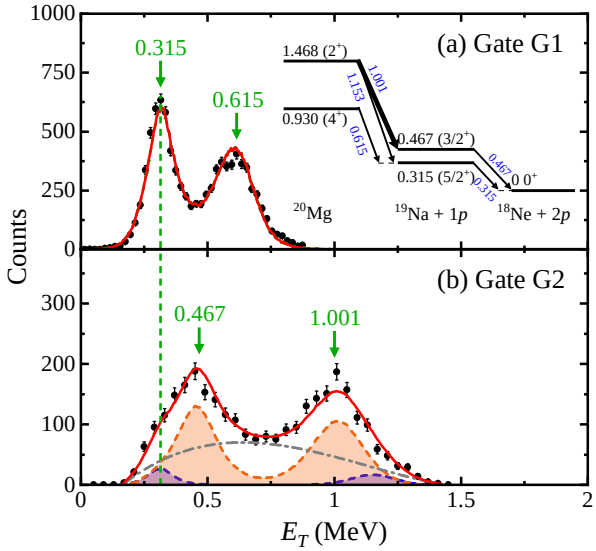


Figure 4. Decay energy E_T spectra for the ^{18}Ne + 1p subsystem with the gates on (**a**) E_T = 0.930 MeV (G1), and (**b**) 1.468 MeV (G2) resonant states in ^{20}Mg [30]. Red lines are the results of simulations, assuming sequential 2p decay for the resonant states in ^{20}Mg resulting from decay paths through the state at E_T = 0.315 MeV in ^{19}Na (dashed-blue curve) and the state at E_T = 0.467 MeV in ^{19}Na (dashed-orange curve). A smooth background (dashed-dotted-grey curve), accounting for 35.2% of the total, is included in (**b**) because of the relatively high background contribution (31.0%) under the E_T = 1.468 MeV state as shown in Figure 3. The green arrows with numbers and dashed-green vertical line show the positions of decay energies in MeV. The inset in (**a**) shows the main decay paths of the first two resonant states in ^{20}Mg. The energies of the states in ^{20}Mg and ^{19}Na relative to the 2p and 1p thresholds, respectively, are listed on the levels in MeV. The energies of the intermediate states in ^{19}Na are consistent with the available experimental results [47–49]. The blue numbers in the inset are the 1p decay energies in MeV between the corresponding states. The bold arrow is the main decay branch of the E_T = 1.468 MeV state in ^{20}Mg.

For the 4_1^+ state at E_T = 0.930 MeV, its ^{18}Ne + 1p subsystem spectrum displays two clear peaks at 0.315 and 0.615 MeV. The lower-energy peak at 0.315 MeV corresponds well to the one-proton decay energy of the ^{19}Na ground state to the ^{18}Ne ground state [see inset in Figure 4a], confirming that the 4_1^+ state in ^{20}Mg decays predominantly via two sequential steps of 1p emission. The first step proceeds to the ground state of ^{19}Na, which subsequently decays to the bound ground state of ^{18}Ne. The red curve in Figure 4a shows the Monte Carlo simulation for this decay path, which agrees well with the experimental data. The 2_2^+ state at E_T = 1.468 MeV exhibits a different decay path. Its ^{18}Ne + 1p subsystem spectrum, shown in Figure 4b, reveals two peaks at 0.467 and 1.001 MeV, respectively. These correspond to two sequential steps of 1p decay via the first excited state of ^{19}Na at E_T = 0.467 MeV [see inset in Figure 4a]. Similar to its ground state, the first excited state of ^{19}Na also decays to the ground state of ^{18}Ne. Further analysis of the subsystem spectrum indicates a minor decay branch for the 2_2^+ state in ^{20}Mg proceeding through the ^{19}Na ground state [blue dashed line in Figure 4b], with a branching ratio of 10.4%. This analysis demonstrates that the distinct decay paths of the first two resonances (4_1^+ and 2_2^+) are consistent with their different spin-parities: the higher-spin 4^+ state favors decay to the $5/2^+$ ground state of ^{19}Na, while the lower-spin 2^+ state decays primarily to the $3/2^+$ first excited state of ^{19}Na. The third resonant state in ^{20}Mg at E_T = 3.008 MeV decays mainly via a sequential 2p emission through the ^{19}Na ground state, similar to the 4_1^+ state, and is not discussed in detail here.

3.3. Three-Proton Decay of ^{21}Al

Recently, Kostyleva et al. observed two resonant states in ^{21}Al via the in-flight decay method [50]. They were tentatively identified as the $5/2^+$ ground state and a low-lying $3/2^+$ excited state, both of which decay by emitting one proton to the ground state of ^{20}Mg. Limited by the insufficient statistics, the $\theta(^{20}\mathrm{Mg}-p)$ angular correlation spectrum in Ref. [50] did not reveal higher-lying resonances. Considering that the two-proton separation energy of ^{20}Mg is only $S_{2p} = 2.418(2)$ MeV [44], higher resonant states in ^{21}Al may become unbound against three-proton emission, decaying via the two-proton unbound states of ^{20}Mg. In this work, ^{21}Al was produced in a transfer reaction where a proton was added to ^{20}Mg and its three-proton decay mechanisms were studied using $^{18}\mathrm{Ne}+3\mathrm{p}$ events [31].

The three-proton decay energy spectrum of ^{21}Al, obtained by invariant mass reconstruction from ^{18}Ne + 3p events, is shown in Figure 5. The corresponding detection efficiency is approximately 10%. Three peaks are suggested, with the first resonance being the most prominent. Their experimental resolutions (FWHM) are 560, 820, and 960 keV, respectively. The decay energies and intrinsic widths of the three resonant states were extracted by fitting the experimental spectrum. For the first resonant state at $E_T = 4.85(5)$ MeV, analysis of the reconstructed kinetic energy distribution confirmed that its population mechanism is consistent with a one-proton transfer reaction. Based on the ab initio valence-space in-medium similarity renormalization group (VS-IMSRG) calculations [51,52], as well as the yields of these high-lying resonant states calculated using the distorted-wave Born approximation (DWBA) method, the spin-parity of the $E_T = 4.85(5)$ MeV resonance in ^{21}Al was assigned as $(1/2^+\text{-}7/2^+)$ [31].

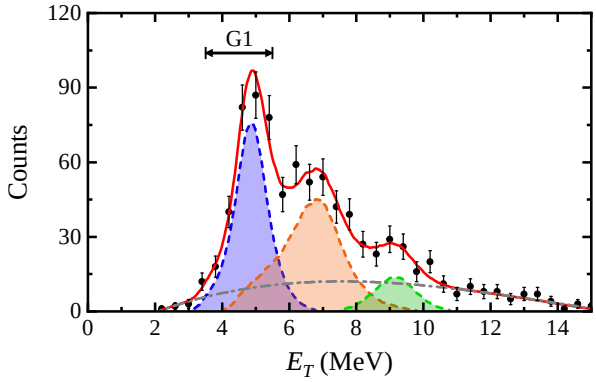


Figure 5. Decay energy E_T spectrum for all detected ^{18}Ne + 3p events [31]. The solid-red curve shows the fitted spectrum along with the contributions of each state (dashed curves) and the smooth background (dashed-dotted-grey curve).

By selecting events corresponding to the $E_T = 4.85(5)$ MeV resonance within the energy gate G1 indicated in Figure 5, the decay energy spectra of its ^{18}Ne + 1p and ^{18}Ne + 2p subsystems were obtained [31], as shown in Figure 6a and Figure 6b, respectively. Within gate G1, the contribution from the smooth background is 14.6%. Three peaks appear in Figure 6a, corresponding to the one-proton decay energies from a three-step sequential decay via the $E_T = 3.008$ MeV intermediate state in ^{20}Mg, following the path 1.84 MeV $\rightarrow$ 2.693 MeV $\rightarrow$ 0.315 MeV (see Figure 7). This indicates a significant decay branch for this resonance proceeding via a sequential three-step 1p decay chain, ultimately decaying to the ground state of ^{18}Ne. Additionally, the counts near 3.92 MeV and 0.615 MeV in Figure 6a correspond to a sequential decay via the $E_T = 0.930$ MeV intermediate state in ^{20}Mg, showing a minor contribution from another sequential decay path: 3.92 MeV $\rightarrow$ 0.615 MeV $\rightarrow$ 0.315 MeV.

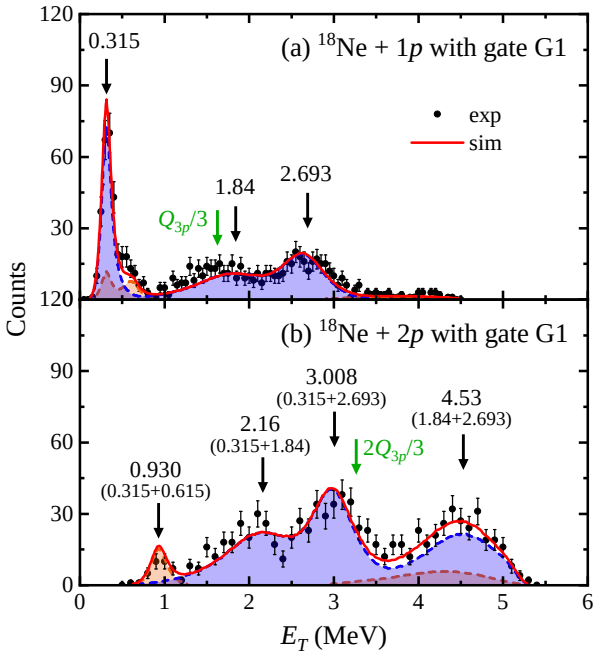


Figure 6. Decay energy E_T spectra for the (**a**) ^{18}Ne + 1p and (**b**) ^{18}Ne + 2p subsystems with the gate G1 on the E_T = 4.85(5) MeV resonant state in ^{21}Al [31]. Red lines are the results of simulations, assuming a three-sequential-steps of 1p decay for the resonant state at E_T = 4.85(5) MeV in ^{21}Al and consisting of simulated results passing through different states in ^{20}Mg (dashed-blue curve corresponds to the decay path via the intermediate state at E_T = 3.008 MeV in ^{20}Mg; dashed-orange curve corresponds to the decay path via the intermediate state at E_T = 0.930 MeV in ^{20}Mg). The black arrows with numbers show the positions of (**a**) 1p decay energies and (**b**) summed energies of two 1p decay energies (in brackets) in MeV. The green arrows are located at (**a**) one-third and (**b**) two-thirds of the total decay energy of the resonant state at E_T = 4.85(5) MeV in ^{21}Al, where the corresponding distribution should peak for prompt 3p decay.

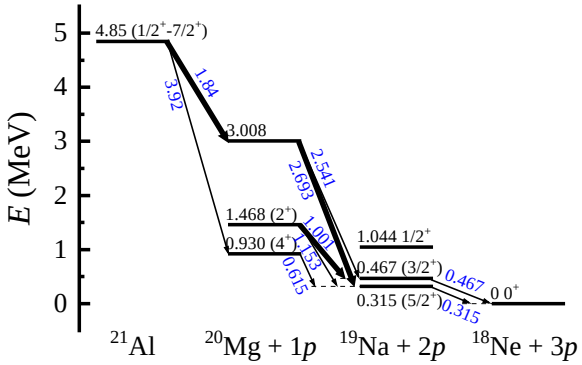


Figure 7. Main decay paths of the resonant state at E_T = 4.85(5) MeV in ^{21}Al [31]. The energies of the states in ^{21}Al, ^{20}Mg, and ^{19}Na relative to the 3p, 2p, and 1p thresholds, respectively, are listed on the levels in MeV. The energies of the intermediate states in ^{20}Mg and ^{19}Na are consistent with the available experimental results [30,47–49]. The blue numbers are the 1p decay energies in MeV between the corresponding states. The bold arrows are the main decay path among the two decay paths of corresponding states.

For the ^{18}Ne + 2p subsystem, pairwise combinations of the three 1p decay energies from the primary decay path yield three summed peaks at 2.16 MeV (0.315 + 1.84), 3.008 MeV (0.315 + 2.693), and 4.53 MeV (1.84 + 2.693). These three summed peaks are clearly seen in Figure 6b. Furthermore, a small peak at 0.930 MeV (0.615 + 0.315) reflects the contribution from the minor decay path (3.92 MeV → 0.615 MeV → 0.315 MeV). The red solid curves in Figure 6a,b represent the results of Monte Carlo simulations for these

two sequential 3p decay paths, with branching ratios of 73.7% and 26.3%, respectively. The experimental spectra of both subsystems are well reproduced by the simulations [31].

It is well known that in prompt 2p decay, the two core + p relative energies are approximately equal, maximizing the product of the barrier penetration factors [53–56]. Consequently, if a prompt 3p decay branch exists for the $E_T = 4.85(5)$ MeV resonance in ^{21}Al, the relative energies between the three protons and the residue are also expected to be roughly equal. This would manifest as peaks near one-third and two-thirds of the total decay energy in the ^{18}Ne + 1p and ^{18}Ne + 2p subsystem spectra, respectively [indicated by green arrows in the Figure 6a,b]. It can be seen that although prompt 3p decay is not the dominant decay mode, the current experimental results cannot entirely rule out the possibility of such a branch existing [31].

3.4. Four-Proton Decay of ^{18}Mg

Recently, we have experimentally observed the isotope ^{18}Mg for the first time, which lies two neutrons beyond the proton drip line [19,57] and represents the second observed case of a four-proton unbound nucleus. Using all measured ^{14}O + 4p coincidence events, whose detection efficiency is approximately 3.5%, the invariant mass spectrum of ^{18}Mg [19] was reconstructed, as shown in Figure 8. Two distinct peaks in the spectrum correspond to two resonant states of ^{18}Mg, with experimental resolutions (FWHM) of 520 keV and 620 keV, respectively. By fitting the experimental spectrum, we obtained the decay energies and intrinsic widths for the ground state and first excited state of ^{18}Mg, which are E_T = 4.865(34) MeV, Γ = 115(100) keV, and E_T = 6.71(14) MeV, Γ = 266(150) keV, respectively. Based on the systematics of the 2^+_1 states in the mirror nucleus ^{18}C and the isotopes ^{20,22}Mg, the observed excited state is identified as the 2^+_1 state of ^{18}Mg [19].

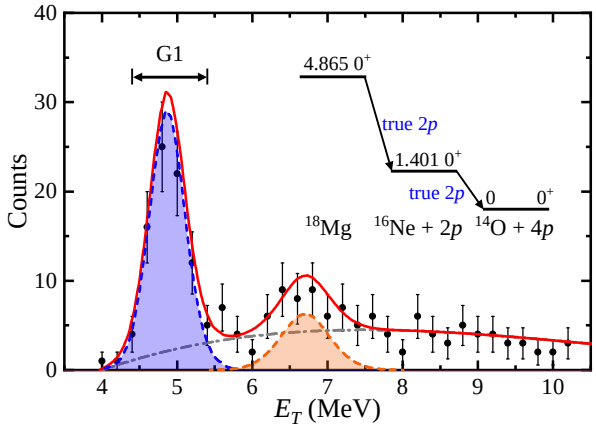


Figure 8. Decay energy E_T spectrum for all detected ^{14}O + 4p events [19]. The solid-red curve shows the fitted spectrum along with the contributions of each state (dashed curves) and the smooth background (dashed-dotted-grey curve). The inset shows the main decay path of the ground state in ^{18}Mg. The energies of the states in ^{18}Mg and ^{16}Ne relative to the 4p and 2p thresholds, respectively, are listed on the levels in MeV. The energies of the resonant states in ^{18}Mg and ^{16}Ne are taken from Refs. [19,58].

To investigate the decay mechanism of the four-proton emission from the ground state of ^{18}Mg, the corresponding events were selected by using the energy gate G1 in Figure 8, within which the background proportion is approximately 17.3%. The relative energy spectrum for its ^{14}O + 2p subsystem was then obtained, which is shown in Figure 9 [19]. It can be seen that the four-proton decay of the ^{18}Mg ground state has significant counts at the position corresponding to the ^{16}Ne ground state, visually indicating that the decay proceeds through the ground state of ^{16}Ne (see inset in Figure 8). It should be noted that there are six possible ways to choose two protons from four. Figure 9 shows the relative

energies of the $^{14}O + 2p$ subsystem calculated for all six combinations. When the ^{18}Mg ground state decays via the ^{16}Ne ground state, only one combination yields the two-proton decay energy of the ^{16}Ne ground state, while the other five combinations constitute the background. Moreover, since the decay energy for the first step of two-proton emission from ^{18}Mg ground state is 3.464 MeV, which is much larger than the 1.401 MeV for the second step from ^{16}Ne ground state, the background from the five incorrect combinations predominantly appears at higher energies in the spectrum. This is clearly reflected in Figure 9, where a narrow peak at around 1.4 MeV corresponds to the two-proton decay energy of the ^{16}Ne ground state, while a broad background at higher energies arises from the five incorrect combinations.

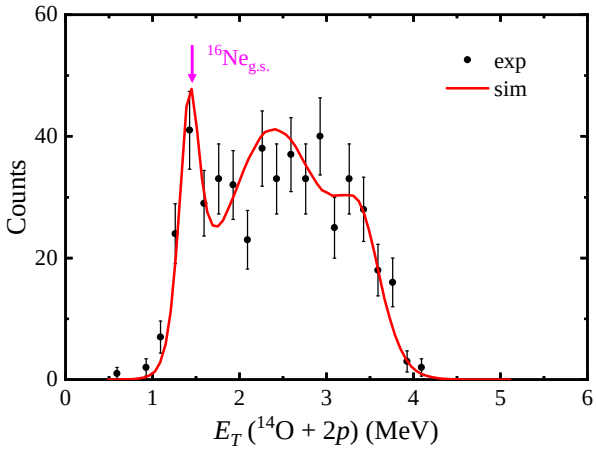


Figure 9. Relative energy E_T spectrum for the $^{14}O + 2p$ subsystem with the gate G1 on $^{18}Mg_{g.s.}$ [19]. Red lines are the results of simulations assuming $^{18}Mg_{g.s.}$ decays to $^{14}O + 4p$ by two sequential steps of prompt $2p$ decay through $^{16}Ne_{g.s.}$, where the decay correlations are assumed to be the same as those observed for $^{16}Ne_{g.s.}$. The arrow shows the decay energy of the ground state of ^{16}Ne.

We further investigated the decay path of the ^{18}Mg ground state using Monte Carlo simulations [19]. The simulations assumed that the ^{18}Mg ground state decays to the ^{14}O ground state via two sequential prompt $2p$ emissions through the intermediate ^{16}Ne ground state. The simulated spectrum, shown as the red curve in Figure 9, agrees well with the experimental data, supporting this proposed decay path. This decay mode is similar to that of ^{8}C. As the first observed four-proton emitter, ^{8}C primarily decays via a two-step cascade of prompt $2p$ emissions through the ground state of ^{6}Be [18]. It is worth noting that ^{28}O, as a four-neutron emitter, also decays mainly via a two-step cascade of prompt $2n$ emissions [59,60], resembling the decay patterns of ^{8}C and ^{18}Mg ground states. In the sequential two-step prompt $2p$ decay of the ^{18}Mg ground state via ^{16}Ne ground state, the two protons emitted in the first step (from ^{18}Mg to ^{16}Ne) most likely share the decay energy of about 1.7 MeV each, and those in the second step (from ^{16}Ne to ^{14}O) about 0.7 MeV each. Thus, when randomly selecting two protons, there is a 2/3 probability of obtaining $E_T(^{14}O + 2p) \approx 1.7 + 0.7 = 2.4$ MeV. Hence, the high counts near 2.4 MeV in Figure 9 do not correspond to a real resonant state in ^{16}Ne, but rather represent a background from incorrect proton combinations. Due to the low statistics for the ^{18}Mg first excited state, it is difficult to determine which resonant state of ^{16}Ne is involved based on the current two-dimensional spectrum analysis and further experimental studies are needed.

4. Conclusions

Investigations of exotic decays and structures of nuclei under extreme conditions of isospin asymmetry have played a pivotal role in revealing new nuclear phenomena and in developing theoretical models, representing one of the most active frontiers in

nuclear physics. Compared to one-nucleon emission, the inherent complexity of multi-nucleon emission can shed more light on the structure and decay mechanisms of drip-line nuclei. This article reviews our recent experimental studies on proton decay in nuclei near the proton drip line around $A \sim 20$. Utilizing the invariant mass method, we investigated the one-proton decay of ^{18}Na, the two-proton decay from excited states of ^{20}Mg, the three-proton decay of ^{21}Al, and the four-proton decay of ^{18}Mg, reconstructing the decay energy spectra for these four nuclei. The ground-state energy of ^{18}Na was determined, clarifying previous controversies regarding its position. Four two-proton resonant states in ^{20}Mg and three three-proton resonant states in ^{21}Al were identified, respectively. Furthermore, the isotope ^{18}Mg, located two neutrons beyond the proton drip line, was observed experimentally for the first time. Through correlation analysis of the decay products from the multi-proton decay processes of ^{20}Mg, ^{21}Al, and ^{18}Mg, combined with Monte Carlo simulations, the decay mechanisms of these resonant states were discussed. The results indicate that the resonant states in ^{20}Mg and ^{21}Al decay predominantly via two-step and three-step sequential $1p$ emission cascades, respectively, while the ground state of ^{18}Mg decays mainly through a two-step sequential prompt $2p$ emission process.

It is important to note that the simultaneous emission of three or more protons has not been experimentally observed to date. All known multi-proton ($\geq$3) decay processes can be described as sequences of sequential $1p$ or $2p$ decays. Whether genuine simultaneous emission of a larger number of protons exists, and how its underlying mechanism might differ from the currently observed $1p$ or $2p$ decay processes, will be a key question for future research on proton decay.

Author Contributions: Conceptualization, L.N. and H.H.; Writing—original draft, L.N.; Writing—review and editing, H.H., Z.L. and Y.J. All authors have read and agreed to the published version of the manuscript.

Funding: This research was funded by the National Key R&D Program of China under Grant No. 2022YFA1602302, and the National Natural Science Foundation of China under Grants No. 12035001 and No. 12535008.

Data Availability Statement: No new data were created or analyzed in this study. Data sharing is not applicable to this article.

Acknowledgments: The authors appreciate the referee for their careful reading of the paper and for their valuable comments.

Conflicts of Interest: The authors declare no conflicts of interest.

Abbreviations

The following abbreviations are used in this manuscript:

Hartree-Fock-Bogoliubov	HFB
Gamow shell model	GSM
Gamow coupled-channel	GCC
NSCL	National Superconducting Cyclotron Laboratory
CCF	Coupled Cyclotron Facility
pps	particles per second
ADSSD	annular double-sided silicon strip detector
SM	shell model
VS-IMSRG	valence-space in-medium similarity renormalization group
DWBA	distorted-wave Born approximation
FWHM	full width at half maximum

References

1. Goldansky, V. On neutron-deficient isotopes of light nuclei and the phenomena of proton and two-proton radioactivity. *Nucl. Phys.* **1960**, *19*, 482–495. [CrossRef]
2. Zel'dovich, Y.B. The Existence of New Isotopes of Light Nuclei and the Equation of State of Neutrons. *Sov. Phys. JETP* **1960**, *38*, 812.
3. Blank, B. One- and Two-Proton Radioactivity. *Lect. Notes Phys.* **2009**, *764*, 153. [CrossRef]
4. Pfützner, M.; Karny, M.; Grigorenko, L.V.; Riisager, K. Radioactive decays at limits of nuclear stability. *Rev. Mod. Phys.* **2012**, *84*, 567–619. [CrossRef]
5. Pfützner, M.; Mukha, I.; Wang, S. Two-proton emission and related phenomena. *Prog. Part. Nucl. Phys.* **2023**, *132*, 104050. [CrossRef]
6. Zhou, L.; Wang, S.M.; Fang, D.Q.; Ma, Y.G. Recent progress in two-proton radioactivity. *Nucl. Sci. Tech.* **2022**, *33*, 105. [CrossRef]
7. Giovinazzo, J.; Blank, B.; Chartier, M.; Czajkowski, S.; Fleury, A.; Lopez Jimenez, M.J.; Pravikoff, M.S.; Thomas, J.C.; de Oliveira Santos, F.; Lewitowicz, M.; et al. Two-Proton Radioactivity of ^{45}Fe. *Phys. Rev. Lett.* **2002**, *89*, 102501. [CrossRef]
8. Pfützner, M.; Badura, E.; Bingham, C.; Blank, B.; Chartier, M.; Geissel, H.; Giovinazzo, J.; Grigorenko, L.V.; Grzywacz, R.; Hellström, M.; et al. First evidence for the two-proton decay of ^{45}Fe. *Eur. Phys. J. A* **2002**, *14*, 279. [CrossRef]
9. Wamers, F.; Marganiec, J.; Aksouh, F.; Aksyutina, Y.; Álvarez-Pol, H.; Aumann, T.; Beceiro-Novo, S.; Boretzky, K.; Borge, M.J.G.; Chartier, M.; et al. First Observation of the Unbound Nucleus ^{15}Ne. *Phys. Rev. Lett.* **2014**, *112*, 132502. [CrossRef]
10. Mukha, I.; Grigorenko, L.V.; Xu, X.; Acosta, L.; Casarejos, E.; Ciemny, A.A.; Dominik, W.; Duénas-Díaz, J.; Dunin, V.; Espino, J.M.; et al. Observation and Spectroscopy of New Proton-Unbound Isotopes ^{30}Ar and ^{29}Cl: An Interplay of Prompt Two-Proton and Sequential Decay. *Phys. Rev. Lett.* **2015**, *115*, 202501. [CrossRef]
11. Goigoux, T.; Ascher, P.; Blank, B.; Gerbaux, M.; Giovinazzo, J.; Grévy, S.; Kurtukian Nieto, T.; Magron, C.; Doornenbal, P.; Kiss, G.G.; et al. Two-Proton Radioactivity of ^{67}Kr. *Phys. Rev. Lett.* **2016**, *117*, 162501. [CrossRef] [PubMed]
12. Webb, T.B.; Wang, S.M.; Brown, K.W.; Charity, R.J.; Elson, J.M.; Barney, J.; Cerizza, G.; Chajecki, Z.; Estee, J.; Hoff, D.E.M.; et al. First Observation of Unbound ^{11}O, the Mirror of the Halo Nucleus ^{11}Li. *Phys. Rev. Lett.* **2019**, *122*, 122501. [CrossRef] [PubMed]
13. Charity, R.J.; Elson, J.M.; Manfredi, J.; Shane, R.; Sobotka, L.G.; Brown, B.A.; Chajecki, Z.; Coupland, D.; Iwasaki, H.; Kilburn, M.; et al. Investigations of three-, four-, and five-particle decay channels of levels in light nuclei created using a ^{9}C beam. *Phys. Rev. C* **2011**, *84*, 014320. [CrossRef]
14. Charity, R.J.; Webb, T.B.; Elson, J.M.; Hoff, D.E.M.; Pruitt, C.D.; Sobotka, L.G.; Brown, K.W.; Cerizza, G.; Estee, J.; Lynch, W.G.; et al. Observation of the Exotic Isotope ^{13}F Located Four Neutrons beyond the Proton Drip Line. *Phys. Rev. Lett.* **2021**, *126*, 132501. [CrossRef]
15. Brown, K.W.; Charity, R.J.; Elson, J.M.; Reviol, W.; Sobotka, L.G.; Buhro, W.W.; Chajecki, Z.; Lynch, W.G.; Manfredi, J.; Shane, R.; et al. Proton-decaying states in light nuclei and the first observation of ^{17}Na. *Phys. Rev. C* **2017**, *95*, 044326. [CrossRef]
16. Xu, X.D.; Mukha, I.; Li, J.G.; Wang, S.M.; Acosta, L.; Bajzek, M.; Casarejos, E.; Cortina-Gil, D.; Espino, J.M.; Fomichev, A.; et al. Isospin Symmetry Breaking Disclosed in the Decay of Three-Proton Emitter ^{20}Al. *Phys. Rev. Lett.* **2025**, *135*, 022502. [CrossRef]
17. Kostyleva, D.; Mukha, I.; Acosta, L.; Casarejos, E.; Chudoba, V.; Ciemny, A.A.; Dominik, W.; Dueñas, J.A.; Dunin, V.; Espino, J.M.; et al. Towards the Limits of Existence of Nuclear Structure: Observation and First Spectroscopy of the Isotope ^{31}K by Measuring Its Three-Proton Decay. *Phys. Rev. Lett.* **2019**, *123*, 092502. [CrossRef]
18. Charity, R.J.; Elson, J.M.; Manfredi, J.; Shane, R.; Sobotka, L.G.; Chajecki, Z.; Coupland, D.; Iwasaki, H.; Kilburn, M.; Lee, J.; et al. $2p$-$2p$ decay of ^{8}C and isospin-allowed $2p$ decay of the isobaric-analog state in ^{8}B. *Phys. Rev. C* **2010**, *82*, 041304. [CrossRef]
19. Jin, Y.; Niu, C.Y.; Brown, K.W.; Li, Z.H.; Hua, H.; Anthony, A.K.; Barney, J.; Charity, R.J.; Crosby, J.; Dell'Aquila, D.; et al. First Observation of the Four-Proton Unbound Nucleus ^{18}Mg. *Phys. Rev. Lett.* **2021**, *127*, 262502. [CrossRef]
20. Charity, R.J.; Wylie, J.; Wang, S.M.; Webb, T.B.; Brown, K.W.; Cerizza, G.; Chajecki, Z.; Elson, J.M.; Estee, J.; Hoff, D.E.M.; et al. Strong Evidence for ^{9}N and the Limits of Existence of Atomic Nuclei. *Phys. Rev. Lett.* **2023**, *131*, 172501. [CrossRef]
21. Olsen, E.; Pfützner, M.; Birge, N.; Brown, M.; Nazarewicz, W.; Perhac, A. Landscape of Two-Proton Radioactivity. *Phys. Rev. Lett.* **2013**, *110*, 222501. [CrossRef]
22. Michel, N.; Nazarewicz, W.; Płoszajczak, M.; Vertse, T. Shell model in the complex energy plane. *J. Phys. G Nucl. Part. Phys.* **2008**, *36*, 013101. [CrossRef]
23. Wang, S.M.; Michel, N.; Nazarewicz, W.; Xu, F.R. Structure and decays of nuclear three-body systems: The Gamow coupled-channel method in Jacobi coordinates. *Phys. Rev. C* **2017**, *96*, 044307. [CrossRef]
24. Berggren, T. On the use of resonant states in eigenfunction expansions of scattering and reaction amplitudes. *Nucl. Phys. A* **1968**, *109*, 265–287. [CrossRef]
25. Michel, N.; Li, J.G.; Xu, F.R.; Zuo, W. Proton decays in ^{16}Ne and ^{18}Mg and isospin-symmetry breaking in carbon isotopes and isotones. *Phys. Rev. C* **2021**, *103*, 044319. [CrossRef]
26. Michel, N.; Li, J.G.; Ru, L.H.; Zuo, W. Calculation of the Thomas-Ehrman shift in ^{16}F and ^{15}O(p,p) cross sections within the Gamow shell model. *Phys. Rev. C* **2022**, *106*, L011301. [CrossRef]

27. Wang, S.M.; Nazarewicz, W. Puzzling Two-Proton Decay of ^{67}Kr. *Phys. Rev. Lett.* **2018**, *120*, 212502. [CrossRef]
28. Wang, S.M.; Nazarewicz, W. Fermion Pair Dynamics in Open Quantum Systems. *Phys. Rev. Lett.* **2021**, *126*, 142501. [CrossRef]
29. Ni, L.; Jin, Y.; Li, Z.H.; Brown, K.W.; Hua, H.; Niu, C.Y.; Anthony, A.K.; Barney, J.; Charity, R.J.; Dell'Aquila, D.; et al. Resonant structure of ^{18}Na and the $N = 8$ shell. *Phys. Rev. C* **2025**, *112*, 024321. [CrossRef]
30. Ni, L.; Jin, Y.; Li, Z.H.; Brown, K.W.; Yuan, C.X.; Hua, H.; Niu, C.Y.; Anthony, A.K.; Barney, J.; Charity, R.J.; et al. Neutron magicity in the proton drip-line nucleus ^{20}Mg: First invariant-mass reconstruction of ^{19,20}Mg. *Phys. Rev. C* **2024**, *110*, L061301. [CrossRef]
31. Ni, L.; Jin, Y.; Li, Z.; Brown, K.; Hua, H.; Niu, C.; Li, J.; Anthony, A.; Barney, J.; Charity, R.; et al. Observation of three-proton-decaying resonant states in ^{21}Al. *Phys. Lett. B* **2025**, *868*, 139660. [CrossRef]
32. Stolz, A.; Baumann, T.; Ginter, T.; Morrissey, D.; Portillo, M.; Sherrill, B.; Steiner, M.; Stetson, J. Production of rare isotope beams with the NSCL fragment separator. *Nucl. Instrum. Methods Phys. Res. Sect. B* **2005**, *241*, 858–861. [CrossRef]
33. Morrissey, D.; Sherrill, B.; Steiner, M.; Stolz, A.; Wiedenhoever, I. Commissioning the A1900 projectile fragment separator. *Nucl. Instrum. Methods Phys. Res. Sect. B* **2003**, *204*, 90–96. [CrossRef]
34. S800 Spectrograph. Available online: https://wikihost.nscl.msu.edu/S800Doc/doku.php?id=introduction (accessed on 26 March 2026).
35. S800 Focal Plane Detector Array. Available online: https://wikihost.nscl.msu.edu/S800Doc/doku.php?id=detectors (accessed on 26 March 2026).
36. Yurkon, J.; Bazin, D.; Benenson, W.; Morrissey, D.; Sherrill, B.; Swan, D.; Swanson, R. Focal plane detector for the S800 high-resolution spectrometer. *Nucl. Instrum. Methods Phys. Res. Sect. A* **1999**, *422*, 291–295. [CrossRef]
37. Bazin, D.; Caggiano, J.; Sherrill, B.; Yurkon, J.; Zeller, A. The S800 spectrograph. *Nucl. Instrum. Methods Phys. Res. Sect. B* **2003**, *204*, 629–633. . [CrossRef]
38. Zerguerras, T.; Blank, B.; Blumenfeld, Y.; Suomijärvi, T.; Beaumel, D.; Brown, B.A.; Chartier, M.; Fallot, M.; Giovinazzo, J.; Jouanne, C.; et al. Study of light proton-rich nuclei by complete kinematics measurements. *Eur. Phys. J. A* **2004**, *20*, 389–396. [CrossRef]
39. Assié, M.; de Oliveira, F.; e521as Collaboration. Spectroscopy of the unbound nucleus ^{18}Na in link with ^{19}Mg two-proton radioactivity. *AIP Conf. Proc.* **2011**, *1409*, 93–97. [CrossRef]
40. Assié, M.; de Oliveira Santos, F.; Davinson, T.; de Grancey, F.; Achouri, L.; Alcántara-Núñez, J.; Al Kalanee, T.; Angélique, J.C.; Borcea, C.; Borcea, R.; et al. Spectroscopy of ^{18}Na: Bridging the two-proton radioactivity of ^{19}Mg. *Phys. Lett. B* **2012**, *712*, 198–202. [CrossRef]
41. Mukha, I.; Grigorenko, L.; Acosta, L.; Alvarez, M.A.G.; Casarejos, E.; Chatillon, A.; Cortina-Gil, D.; Espino, J.M.; Fomichev, A.; García-Ramos, J.E.; et al. New states in ^{18}Na and ^{19}Mg observed in the two-proton decay of ^{19}Mg. *Phys. Rev. C* **2012**, *85*, 044325. [CrossRef]
42. Charity, R.J.; Brown, K.; Webb, T.; Sobotka, L.G. Invariant-mass spectroscopy of ^{10}B,^{11} C,^{14} F,^{16} F, and ^{18}Na. *Phys. Rev. C* **2023**, *107*, 054301. [CrossRef]
43. Mukha, I.; Sümmerer, K.; Acosta, L.; Alvarez, M.A.G.; Casarejos, E.; Chatillon, A.; Cortina-Gil, D.; Espino, J.; Fomichev, A.; García-Ramos, J.E.; et al. Observation of Two-Proton Radioactivity of ^{19}Mg by Tracking the Decay Products. *Phys. Rev. Lett.* **2007**, *99*, 182501. [CrossRef]
44. Wang, M.; Huang, W.; Kondev, F.; Audi, G.; Naimi, S. The AME 2020 atomic mass evaluation (II). Tables, graphs and references. *Chin. Phys. C* **2021**, *45*, 030003. [CrossRef]
45. Randhawa, J.S.; Kanungo, R.; Holl, M.; Holt, J.D.; Navrátil, P.; Stroberg, S.R.; Hagen, G.; Jansen, G.R.; Alcorta, M.; Andreoiu, C.; et al. Observation of excited states in ^{20}Mg sheds light on nuclear forces and shell evolution. *Phys. Rev. C* **2019**, *99*, 021301(R). [CrossRef]
46. LaFrance, S.; Fortune, H.T.; Mordechai, S.; Cobern, M.E.; Moore, G.E.; Middleton, R.; Chung, W.; Wildenthal, B.H. ^{20}O from ^{18}O(t,p). *Phys. Rev. C* **1979**, *20*, 1673–1679. [CrossRef]
47. Benenson, W.; Guichard, A.; Kashy, E.; Mueller, D.; Nann, H.; Robinson, L. Mass measurements of ^{19}Na and ^{23}Al using the (^{3}He, ^{8}Li) reaction. *Phys. Lett. B* **1975**, *58*, 46–48. [CrossRef]
48. Angulo, C.; Tabacaru, G.; Couder, M.; Gaelens, M.; Leleux, P.; Ninane, A.; Vanderbist, F.; Davinson, T.; Woods, P.J.; Schweitzer, J.S.; et al. Identification of a new low-lying state in the proton drip line nucleus ^{19}Na. *Phys. Rev. C* **2003**, *67*, 014308. [CrossRef]
49. Mukha, I.; Sümmerer, K.; Acosta, L.; Alvarez, M.A.G.; Casarejos, E.; Chatillon, A.; Cortina-Gil, D.; Egorova, I.A.; Espino, J.M.; Fomichev, A.; et al. Spectroscopy of proton-unbound nuclei by tracking their decay products in-flight: One- and two- proton decays of ^{15}F, ^{16}Ne, and ^{19}Na. *Phys. Rev. C* **2010**, *82*, 054315. [CrossRef]
50. Kostyleva, D.; Xu, X.D.; Mukha, I.; Acosta, L.; Bajzek, M.; Casarejos, E.; Ciemny, A.A.; Cortina-Gil, D.; Dominik, W.; Dueñas, J.A.; et al. Observation and spectroscopy of the proton-unbound nucleus ^{21}Al. *Phys. Rev. C* **2024**, *110*, L031301. [CrossRef]
51. Li, H.H.; Li, J.G.; Xie, M.R.; Zuo, W. Ab initio calculations of mirror energy difference in sd-shell nuclei*. *Chin. Phys. C* **2023**, *47*, 124101. [CrossRef]
52. Xu, X.Y.; Fan, S.Q.; Yuan, Q.; Hu, B.S.; Li, J.G.; Wang, S.M.; Xu, F.R. Progress in *ab initio* in-medium similarity renormalization group and coupled-channel method with coupling to the continuum. *Nucl. Sci. Tech.* **2024**, *35*, 215. [CrossRef]

53. Egorova, I.A.; Charity, R.J.; Grigorenko, L.V.; Chajecki, Z.; Coupland, D.; Elson, J.M.; Ghosh, T.K.; Howard, M.E.; Iwasaki, H.; Kilburn, M.; et al. Democratic Decay of ^{6}Be Exposed by Correlations. *Phys. Rev. Lett.* **2012**, *109*, 202502. [CrossRef]
54. Brown, K.W.; Charity, R.J.; Sobotka, L.G.; Chajecki, Z.; Grigorenko, L.V.; Egorova, I.A.; Parfenova, Y.L.; Zhukov, M.V.; Bedoor, S.; Buhro, W.W.; et al. Observation of Long-Range Three-Body Coulomb Effects in the Decay of ^{16}Ne. *Phys. Rev. Lett.* **2014**, *113*, 232501. [CrossRef]
55. Webb, T.B.; Charity, R.J.; Elson, J.M.; Hoff, D.E.M.; Pruitt, C.D.; Sobotka, L.G.; Brown, K.W.; Barney, J.; Cerizza, G.; Estee, J.; et al. Particle decays of levels in ^{11,12}N and ^{12}O investigated with the invariant-mass method. *Phys. Rev. C* **2019**, *100*, 024306. [CrossRef]
56. Miernik, K.; Dominik, W.; Janas, Z.; Pfützner, M.; Grigorenko, L.; Bingham, C.R.; Czyrkowski, H.; Ćwiok, M.; Darby, I.G.; Dąbrowski, R.; et al. Two-Proton Correlations in the Decay of ^{45}Fe. *Phys. Rev. Lett.* **2007**, *99*, 192501. [CrossRef]
57. Zhou, L.; Fang, D.Q.; Wang, S.M.; Hua, H. Structure and 2p decay mechanism of ^{18}Mg. *Nucl. Sci. Tech.* **2024**, *35*, 107. [CrossRef]
58. NNDC. Available online: https://www.nndc.bnl.gov/ensdf/ (accessed on 26 March 2026).
59. Kondo, Y.; Achouri, N.L.; Al Falou, H.; Atar, L.; Aumann, T.; Baba, H.; Boretzky, K.; Caesar, C.; Calvet, D.; Chae, H.; et al. First observation of ^{28}O. *Nature* **2023**, *620*, 965–970. [CrossRef]
60. Li, J.G.; Hu, B.S.; Zhang, S.; Xu, F.R. Unbound ^{28}O, the heaviest oxygen isotope observed: A cutting-edge probe for testing nuclear models. *Nucl. Sci. Tech.* **2024**, *35*, 21. [CrossRef]

Disclaimer/Publisher's Note: The statements, opinions and data contained in all publications are solely those of the individual author(s) and contributor(s) and not of MDPI and/or the editor(s). MDPI and/or the editor(s) disclaim responsibility for any injury to people or property resulting from any ideas, methods, instructions or products referred to in the content.